



RESEARCH LETTER

10.1002/2014GL060811

Key Points:

- Monsoon precipitation decrease over the second half of the twentieth century
- Decrease in precipitation can only be explained by anthropogenic aerosol
- This result is consistent across all Northern Hemisphere monsoon regions

Supporting Information:

- Readme
- Supplementary material (Table S1 and Figures S1–S14)

Correspondence to:

D. Polson,
dpolson@staffmail.ed.ac.uk

Citation:

Polson, D., M. Bollasina, G. C. Hegerl, and L. J. Wilcox (2014), Decreased monsoon precipitation in the Northern Hemisphere due to anthropogenic aerosols, *Geophys. Res. Lett.*, *41*, 6023–6029, doi:10.1002/2014GL060811.

Received 6 JUN 2014

Accepted 29 JUL 2014

Accepted article online 3 AUG 2014

Published online 19 AUG 2014

This is an open access article under the terms of the Creative Commons Attribution License, which permits use, distribution and reproduction in any medium, provided the original work is properly cited.

Decreased monsoon precipitation in the Northern Hemisphere due to anthropogenic aerosols

D. Polson¹, M. Bollasina¹, G. C. Hegerl¹, and L. J. Wilcox²

¹School of GeoSciences, Grant Institute, University of Edinburgh, Edinburgh, UK, ²National Centre for Atmospheric Science (Climate), Department of Meteorology, University of Reading, Reading, UK

Abstract The Northern Hemisphere monsoons are an integral component of Earth's hydrological cycle and affect the lives of billions of people. Observed precipitation in the monsoon regions underwent substantial changes during the second half of the twentieth century, with drying from the 1950s to mid-1980s and increasing precipitation in recent decades. Modeling studies suggest that anthropogenic aerosols have been a key factor driving changes in tropical and monsoon precipitation. Here we apply detection and attribution methods to determine whether observed changes are driven by human influences using fingerprints of individual forcings (i.e., greenhouse gas, anthropogenic aerosol, and natural) derived from climate models. The results show that the observed changes can only be explained when including the influence of anthropogenic aerosols, even after accounting for internal climate variability. Anthropogenic aerosol, not greenhouse gas or natural forcing, has been the dominant influence on Northern Hemisphere monsoon precipitation over the second half of the twentieth century.

1. Introduction

Human-induced changes to the hydrological cycle are among the most serious impacts of climate change, with potential consequences for water resources, health, agriculture, and ecosystems worldwide. Warming of the atmosphere due to increasing greenhouse gas concentrations causes atmospheric water vapor to increase in line with the Clausius Clapeyron relationship at $\sim 7\% \text{ K}^{-1}$ [Held and Soden, 2006; Willett et al., 2010]. Consequently, global precipitation also increases, though at a lower rate ($\sim 2\% \text{ K}^{-1}$) due to energy balance constraints [Allen and Ingram, 2002; Trenberth et al., 2003]. Increasing moisture transport is expected to enhance the existing pattern of precipitation minus evaporation, with increasing tropical and decreasing subtropical precipitation [Held and Soden, 2006; Seager and Naik, 2012]. The increase in precipitation due to warming is partly offset by anthropogenic aerosols. Aerosols scatter and absorb incoming solar radiation, causing cooling at the surface and heating of the atmosphere [Ming and Ramaswamy, 2009]. Aerosols also influence precipitation by interacting with clouds [Rotstayn and Lohmann, 2002], and models that include this process tend to better reproduce observed temperature and precipitation records of the twentieth century [Wilcox et al., 2013]. The asymmetrical cooling from aerosols between the Northern and Southern Hemispheres also affects tropical precipitation by causing a southward shift of the Intertropical Convergence Zone [Rotstayn and Lohmann, 2002; Ackerley et al., 2011; Hwang et al., 2013].

The counteracting effects of greenhouse gases and aerosols on precipitation, and the similar spatial response patterns, can make distinguishing their influence challenging [Xie et al., 2013]. Detection and attribution studies have shown that greenhouse gas forcing has influenced changes in global precipitation [Polson et al., 2013a, 2013b; Wu et al., 2013]. These studies attribute observed changes to individual forcings using statistical analysis techniques that account for the internal variability of the climate. However, the influence of aerosols has yet to be separated from the combined anthropogenic forcing [Zhang et al., 2007; Polson et al., 2013b] or the combined influence of all nongreenhouse gas forcings, though this is assumed to be dominated by aerosols [Wu et al., 2013]. Anthropogenic aerosol emissions rapidly increased from the 1950s (Figure 1) and are thought to have contributed to a reduction in precipitation in monsoon regions in Africa [Held et al., 2005] and Asia [Lau and Kim, 2006; Meehl et al., 2008; Guo et al., 2013]. Climate models that include anthropogenic aerosol forcing better reproduce the observed decrease in South Asian monsoon precipitation [Bollasina et al., 2011]. Here we investigate the influence of individual forcings on summer monsoon land precipitation for the whole Northern Hemisphere during 1951–2005, for which there are reliable long-term observational records. By analyzing the Northern Hemisphere monsoon system as a whole, rather than its regional manifestations, we can more easily identify how external forcings have affected this

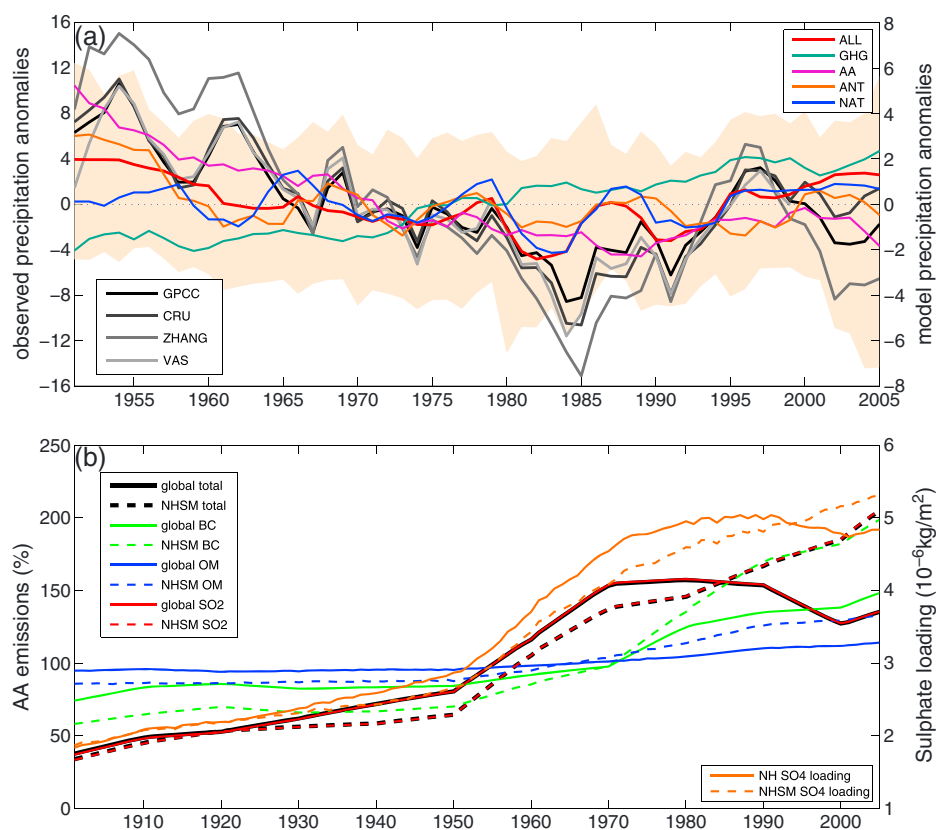


Figure 1. (a) May–September NHSM precipitation anomalies (mm/month) for 1951–2005 for observational data sets, CRU, GPCCC, Zhang, and VasClimO (VasClimO is 1951–2000). Multimodel mean anomalies (different scale to observations) are for all external forcings (ALL), greenhouse gas (GHG), anthropogenic aerosol (AA), natural (NAT), and anthropogenic (ANT) forcing. Anomalies are with respect to 1951–2005 and smoothed with a 5 year running mean. Orange shading shows the ALL ensemble 5%–95% range (same scale as observations). Models are masked to the GPCCC data set. (b) Global and NHSM annual anthropogenic aerosol emissions (% of 1901–2005 mean emissions). NHSM emissions are for 0° – 40° N. Total is BC + OM + SO₂, BC is black carbon, OM is organic matter, and SO₂ is sulfur dioxide. The annual sulfate loadings for the NH and NHSM region are also shown. Aerosol emissions are the CMIP5 emissions based on Lamarque *et al.* [2010], and sulfate loading is the mean of 11 climate models.

important component of the global overturning circulation. Detection and attribution [Allen and Stott, 2003] provides a unique and rigorous technique to ascertain whether the observed changes can be explained by internal climate variability alone or whether external forcing has played a role in driving the changes. Previous studies of monsoon precipitation are limited to individual models or do not make use of such rigorous statistical methods. In this study, large climate model ensembles are used to derive “fingerprints” of forcing for individual and combined external forcings. Detection and attribution methods are applied to determine which forcing, if any, can explain the observed changes.

2. Data: Observations and Models

Four observational data sets were used to calculate the mean summer (May–September) precipitation anomalies in Northern Hemisphere summer monsoon (NHSM) region: CRUTS3.21 (CRU) [Harris *et al.*, 2014], Global Precipitation Climatology Centre (GPCCC) [Schneider *et al.*, 2014], VasclimO [Beck *et al.*, 2005], and an updated version of the data set from Zhang *et al.* [2007]. Each data set is aggregated to the same $5^{\circ} \times 5^{\circ}$ grid, which is the lowest resolution among them. A grid box is only included in the analysis if over 70% of the grid box is land and if it has coverage in over 90% of years.

Multimodel ensembles of climate model simulations from the Climate Model Intercomparison Project 5 (CMIP5) archive were used to derive response patterns to various forcings including all external forcings (ALL), which combines anthropogenic (greenhouse gases, aerosols, land use, and ozone) and natural forcings (volcanic and solar), greenhouse gas forcing (GHG), anthropogenic aerosol forcing (AA), natural forcing (NAT), and all anthropogenic forcings (ANT) (Table S1 in the supporting information).

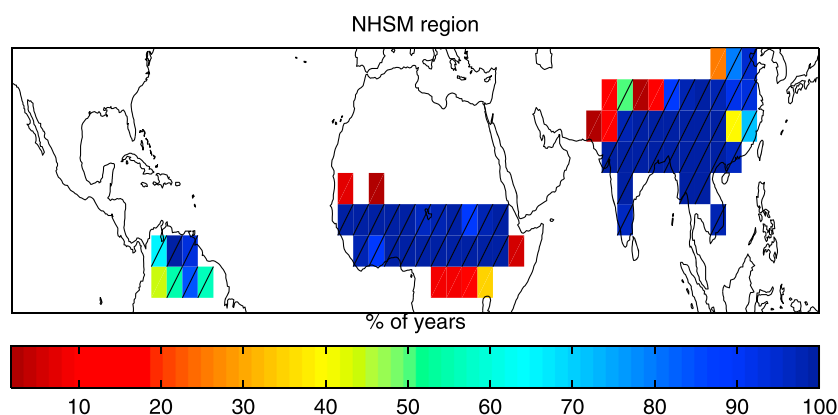


Figure 2. Northern Hemisphere summer monsoon region for GPCP. Percentage of years a grid box meets the NHSM precipitation criteria for GPCP data set. Hatched areas show grid boxes defined in NHSM region based on mean annual range and May to September precipitation for all years in 1951–2005.

3. Northern Hemisphere Summer Monsoon Region

Following *Hsu et al.* [2011], the NHSM region encloses grid boxes for which the mean annual range (difference between the May–September and November–March averages) in precipitation for all years exceeds 2 mm d^{-1} and the mean May–September precipitation exceeds 55% of the annual total. Grid boxes are excluded if they are north of the subtropics (40°N) or isolated. The region is fixed for all years; therefore, any spatial shift of the monsoon is not captured. However, changes in precipitation due to possible variations in the monsoon area should be small compared to the total precipitation in the whole region. Figure 2 shows that the NHSM region does not change by much over the observation period, with only a few grid boxes that meet the criteria in at least 1 year excluded from the final NHSM mask. An alternative method would allow the region to change year by year, but this could result in the region changing size, making it difficult to distinguish changes in precipitation rate from changes due to the NHSM region shrinking or growing over time. The NHSM region is defined for each observational data set, and the model data are masked to match the spatial and temporal coverage of each.

4. Detection and Attribution

The 1951–2005 time series for the mean May–September precipitation anomalies (with respect to the mean for 1951–2005, 2000 for the VasclimO data set) are calculated for the NHSM region. The analysis ends in 2005 as many historical model simulations do not run beyond that year. A 5 year running mean is applied to smooth the data prior to analysis, and the smoothed time series are used in a total least squares regression [Allen and Stott, 2003]. The model-derived fingerprints of forcing, \mathbf{F} , are scaled to the observations, \mathbf{y} , to estimate the contribution of p forcings to the NHSM precipitation using

$$\mathbf{y} = (\mathbf{F} + \varepsilon_{\text{finger}})\beta + \varepsilon_{\text{noise}} \quad (1)$$

where \mathbf{F} is a $l \times p$ matrix for p forcing fingerprints of length l representing time and \mathbf{y} is a rank- l vector representing the observed monsoon precipitation change; β is a vector of scaling factors with p entries giving the magnitude of each fingerprint in the observations, $\varepsilon_{\text{noise}}$ is the residual associated with internal climate variability, and $\varepsilon_{\text{finger}}$ is variability that remains in the fingerprint after multimodel averaging.

To ensure that the observations cannot be explained by internal climate variability alone, multiple samples of climate noise, estimated from the model internal variability, are added to the noise-reduced $\tilde{\mathbf{F}}$ and $\tilde{\mathbf{y}}$ (see below), and β is recalculated. If $\beta > 0$ at 5% significance level, then the fingerprint response pattern is detected in the observations [Hegerl and Zwiers, 2011]. If $0 < \beta < 1$, the models overestimate the observations, and if $\beta > 1$ then the models underestimate observations. Because climate models tend to underestimate the observed variability in precipitation (Figure S14 in the supporting information), the model variance is doubled when calculating the noise samples.

Best estimates of the noise-reduced observations and model fingerprints are calculated using

$$\tilde{\mathbf{Z}} = \mathbf{Z} - \mathbf{Z}\tilde{\mathbf{v}}\tilde{\mathbf{v}}^T \quad (2)$$

where $\mathbf{Z} \equiv [\mathbf{F}, \mathbf{y}]$ and $\bar{\mathbf{v}}$ contains the eigenvector coefficients used to calculate β when solving equation (1). The robustness of the result is assessed by comparing the regression residual, ϵ_{noise} , to samples of model variability using the F test described in *Allen and Stott* [2003].

In this analysis the noise samples are taken from the greenhouse gas only ensemble by subtracting the multimodel mean from each individual model simulation and multiplying by $\sqrt{\frac{n}{n-1}}$, where n is the number of simulations in the ensemble, to avoid bias in the variance. The estimate of internal variability should not be sensitive to the choice of a specific ensemble, and though the ALL-forced ensemble would provide the most samples of noise, practical computational limitations prohibited its use (note that use of the ALL ensemble for the one-signal and two-signal analyses yielded very similar results). The ALL ensemble was used to calculate samples of noise for the residual consistency check. All the results presented here are based on nonoptimized fingerprints. While optimizing the fingerprints using the internal variability covariance matrix can enhance detectability, it also complicates interpretation by requiring truncation to a lower dimensional space. See *Allen and Stott* [2003] for more details.

The ALL fingerprint is regressed onto the observation in a one-signal analysis to determine whether external forcing is detectable in the observations. To separately investigate the aerosol impact on radiation (direct effect) and the effect on clouds (indirect effect), the ALL forced models are also divided into two groups, those that include both effects and those that include the direct effect only (see Table S1 and Figure S3). The ALL fingerprint is a combination of a number of different individual forcings that for the whole NHSM region add approximately linearly in models (supporting information). A two-signal analysis was applied to distinguish the role of these individual forcings in driving the observed changes by simultaneously regressing ANT and NAT, AA and GHG, AA and NAT, and GHG and NAT fingerprints onto the observations. We also apply a further test by simultaneously regressing the AA, GHG, and NAT fingerprints onto observations in a three-signal analysis. For the two-signal and three-signal analyses, all available models were used to produce the fingerprints of forcing, meaning that a different number of simulations and different models were used for different forcings. To ensure this did not influence the results, the detection and attribution analysis was repeated with the same models used to produce the fingerprints in each pair of forcings for the two-signal analysis and the GHG, NAT, and AA fingerprints for the three-signal analysis. The detection results were the same for all cases regardless of the ensemble used to produce the fingerprints (see Figure S12 in the supporting information). The residual consistency check passes for all results presented here except for one case where the ALL fingerprint is regressed onto the Zhang observational data (highlighted in the Figure 3 caption).

5. Results

The observed 1951–2005 monsoon precipitation anomalies show a distinctive drying pattern from 1951 to the mid-1980s, followed by increasing precipitation until 2000 (Figure 1a). During 2000–2005, there is a striking inconsistency among the available observational data sets, likely due to the drop in the number of stations during this period [*Schneider et al.*, 2014]. Nevertheless, all observational data sets show a decrease in precipitation from 1951 to 2005; fitting linear trends gives an overall decrease of 5%–11% of the mean precipitation, depending on the data set.

Including anthropogenic aerosols substantially improves models' ability to reproduce the observations. The precipitation changes (Figure 1a) of the ALL, ANT, and AA multimodel means have the same general behavior as observations, with decreasing precipitation from 1951 to mid-1980s, followed by a recovery during the 1990s. In contrast to observations, the GHG multimodel mean shows precipitation consistently increasing during this period. The NAT multimodel mean has no overall trend but has short-term drying following volcanic eruptions.

The signature of anthropogenic forcing is distinctly recognizable over other forcings and is mostly associated with aerosols. While the ALL and ANT multimodel mean unsmoothed time series correlate with AA (0.23 and 0.36, respectively, p value < 0.1), GHG is negatively correlated with both ALL and ANT (–0.2 in both cases). ALL and ANT also resemble the observations (correlation > 0.3 and p values < 0.05 in all but one case). AA is positively correlated with observations, while GHG and observations are negatively correlated. Spatial linear trend patterns also show more similarity between observed, ALL, ANT, and AA, which show drying in many areas, than GHG which results in increasing precipitation over most of the NHSM region (Figure S2 in the supporting information).

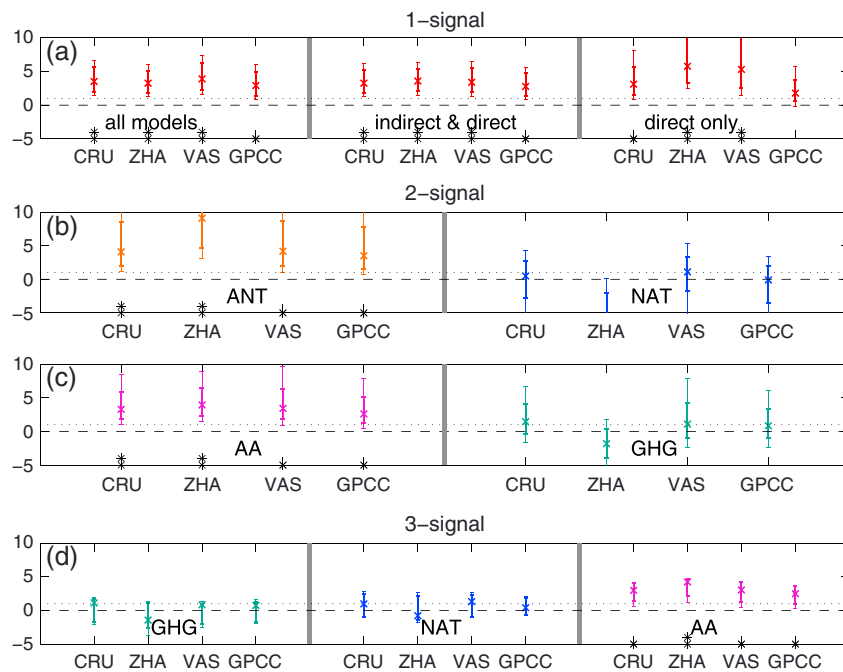


Figure 3. Detection and attribution of observed changes in Northern Hemisphere summer monsoon precipitation. (a) One-signal regression for all external forcings (ALL), all external forcings for models with indirect and direct effects, and all external forcings for models with direct effect only. (b) Two-signal regression for anthropogenic (ANT) and natural (NAT) forcing. (c) Two-signal regression for anthropogenic aerosol (AA) and greenhouse gas (GHG) forcing. (d) Three-signal regression for greenhouse gas (GHG), natural (NAT), and anthropogenic aerosol (AA) forcing. Results are shown for four observational data sets, CRU (CRU), Zhang (ZHA), VasClimO (VAS), and GPCC (GPCC). Crosses show the best guess scaling factor for the multimodel mean, thick lines are the 90% confidence interval based on the raw variance, and thin lines are the 90% confidence intervals when model variance has been doubled. The residual consistency test is passed, except for one-signal ALL analysis for ZHA. Stars show where forcing is detected, and two stars show where forcing is detected but inconsistent with a scaling factor of 1.

That aerosols may be a key factor implicated in the twentieth century monsoon precipitation changes is also suggested by increasing global aerosol emissions from the 1950s to mid-1980s, followed by a period of decreasing emissions (Figure 1b), which mirrors the changes in precipitation, though local emissions continue to increase during this period. This hints that aerosols from remote sources also contribute to the NHSM changes, as several studies have suggested to be the case for the Asian monsoon [see, e.g., Cowan and Cai, 2011]. However, it is not possible to quantify the relative influence of remote and local emissions from the analysis in this paper.

Results for the detection and attribution analysis confirm that external forcing has played a substantial role in driving the observed changes. When the ALL fingerprint is scaled to the observations, we find that it is detectable (Figure 3a) and larger than simulated in models (scaling factors of around 3 to 4). Repeating the regression for direct effect and indirect effect groups suggests that at least in the CMIP5 models, inclusion of the indirect effect does not significantly improve detection and attribution results (Figure 3a). However, different spatial trend patterns suggest that the indirect effect does play an important role over parts of Asia. Models that include the indirect effect tend to simulate more drying than models that only include the direct effect (Figure S2 in the supporting information). We add a note of caution that currently models still have limited representation of the indirect effect, which additionally can lead to counteracting changes [Stevens and Feingold, 2009].

Simultaneous regression of the ANT and NAT fingerprints onto the observations shows that while the ANT fingerprint is detectable, NAT cannot be distinguished from internal climate variability (Figure 3b). Results for AA and GHG, AA and NAT, and GHG and NAT show that anthropogenic aerosol forcing is largely responsible for changes in NHSM precipitation, with its fingerprint detectable in observations (when estimated against GHG, NAT; Figures 3c and S1), while those of other forcings generally are not. GHG estimated against NAT yields a detectable NAT signal in some cases.

Simultaneously regressing the AA, GHG, and NAT fingerprints onto observations in a three-signal analysis (Figure 3d) confirms that anthropogenic aerosol forcing, which is detectable in observations, is driving changes in NHSM precipitation, while the influence of greenhouse gas and natural forcing cannot be distinguished from internal climate variability.

Given the significance of the detected signal for the whole NHSM region, we tested if all regions contributed to this finding or if it is attributable to one specific region. The analysis was repeated excluding first South America (Figure S11a in the supporting information), then Africa (Figure S11b in the supporting information), and finally Asia (Figure S11c in the supporting information). The results show that the detection of anthropogenic aerosol forcing is largely insensitive to the exclusion of any one region. The detection and attribution results were also not affected by including the midlatitude sector of the NHSM region (Figure S11d in the supporting information).

6. Discussion and Conclusions

Northern Hemisphere monsoon precipitation underwent substantial changes during the second half of the twentieth century. Climate models suggest that increasing greenhouse gas concentrations alone would have caused an increase in precipitation during this period. However, this is more than offset by the influence of anthropogenic aerosols, resulting in a decrease in precipitation over the last 50 years. Internal climate variability is also likely to have played a role in driving the observed changes. As temperatures in the Atlantic ocean have been shown to influence Northern Hemisphere monsoon precipitation [Chiang and Friedman, 2012], studies of multidecadal temperature variability in the tropical North Atlantic suggest internal climate variability to be important [Zhang et al., 2013]. Satellite observations of precipitation over both land and ocean show an intensification of monsoon precipitation over the last 30 years [Hsu et al., 2011] which has also been linked to climate variability such as El Niño-Southern Oscillation [Wang et al., 2013]. However, the analysis in this paper shows that the influence of anthropogenic aerosol forcing on NHSM precipitation is detectable above this internal climate variability. It provides compelling evidence that anthropogenic aerosols are the dominant external factor influencing the observed changes in NHSM precipitation over the second half of the twentieth century and that these changes cannot be explained by greenhouse gas forcing, natural forcing, or by internal climate variability alone.

Acknowledgments

The authors acknowledge the use of precipitation data of the VasClimO project, the Global Precipitation Climatology Centre, The Global Historical Climatology Network and Xuebin Zhang, and the Climatic Research Unit. We thank the World Climate Research Programme's Working Group on Coupled Modelling, the climate modeling groups (Table S1), the U.S. Department of Energy's Program for Climate Model Diagnosis and Intercomparison, and the Global Organization for Earth System Science Portals and thank the reviewers for their useful comments. This work was supported by the NERC project PAGODA (NE/I006672/1) and ERC funded project (EC-320691) TITAN, the National Science Foundation (ATM-0296007), NCAS, the U.S. Department of Energy's Office of Science, and NOAA's Climate Program Office.

The Editor thanks Jinqiang Chen and an anonymous reviewer for their assistance in evaluating this paper.

References

- Ackerley, D., B. B. Booth, S. H. E. Knight, E. J. Highwood, D. J. Frame, M. R. Allen, and D. P. Rowell (2011), Sensitivity of twentieth-century Sahel rainfall to sulfate aerosol and CO₂ forcing, *J. Clim.*, *24*(19), 4999–5014.
- Allen, M., and W. Ingram (2002), Constraints on future changes in climate and the hydrologic cycle, *Nature*, *419*(6903), 224–232.
- Allen, M., and P. Stott (2003), Estimating signal amplitudes in optimal fingerprinting. Part I: Theory, *Clim. Dyn.*, *21*(5), 477–491.
- Beck, C., J. Grieser, and B. Rudolf (2005), A new monthly precipitation climatology for the global land areas for the period 1951 to 2000, *Climate Status Report 2004*, German Weather Service, Offenbach, Germany.
- Bollasina, M. A., Y. Ming, and V. Ramaswamy (2011), Anthropogenic aerosols and the weakening of the south Asian summer monsoon, *Science*, *334*(6055), 502–505.
- Chiang, J. C. H., and A. R. Friedman (2012), Extratropical cooling, interhemispheric thermal gradients, and tropical climate change, *Annu. Rev. Earth Planet. Sci.*, *40*(1), 383–412.
- Cowan, T., and W. Cai (2011), The impact of Asian and non-Asian anthropogenic aerosols on 20th century Asian summer monsoon, *Geophys. Res. Lett.*, *38*, L11703, doi:10.1029/2011GL047268.
- Guo, L., E. J. Highwood, L. C. Shaffrey, and A. G. Turner (2013), The effect of regional changes in anthropogenic aerosols on rainfall of the east Asian summer monsoon, *Atmos. Chem. Phys.*, *13*(3), 1521–1534.
- Harris, I., P. Jones, T. Osborn, and D. Lister (2014), Updated high-resolution grids of monthly climatic observations—The CRU ts3.10 dataset, *Int. J. Climatol.*, *34*, 623–642.
- Hegerl, G., and F. Zwiers (2011), Use of models in detection and attribution of climate change, *Wiley Interdiscip. Rev. Clim. Change*, *2*(4), 570–591.
- Held, I., and B. Soden (2006), Robust responses of the hydrological cycle to global warming, *J. Clim.*, *19*(21), 5686–5699.
- Held, I., T. Delworth, J. Lu, K. Findell, and T. Knutson (2005), Simulation of Sahel drought in the 20th and 21st centuries, *Proc. Natl. Acad. Sci.*, *102*(50), 17,891–17,896.
- Hsu, P.-C., T. Li, and B. Wang (2011), Trends in global monsoon area and precipitation over the past 30 years, *Geophys. Res. Lett.*, *38*, L08701, doi:10.1029/2011GL046893.
- Hwang, Y.-T., D. M. W. Frierson, and S. M. Kang (2013), Anthropogenic sulfate aerosol and the southward shift of tropical precipitation in the late 20th century, *Geophys. Res. Lett.*, *40*, 2845–2850, doi:10.1002/grl.50502.
- Lamarque, J.-F., et al. (2010), Historical (1850–2000) gridded anthropogenic and biomass burning emissions of reactive gases and aerosols: Methodology and application, *Atmos. Chem. Phys.*, *10*(15), 7017–7039.
- Lau, K.-M., and K.-M. Kim (2006), Observational relationships between aerosol and Asian monsoon rainfall, and circulation, *Geophys. Res. Lett.*, *33*, L21810, doi:10.1029/2006GL027546.
- Meehl, G. A., J. M. Arblaster, and W. D. Collins (2008), Effects of black carbon aerosols on the Indian monsoon, *J. Clim.*, *21*(12), 2869–2882.
- Ming, Y., and V. Ramaswamy (2009), Nonlinear climate and hydrological responses to aerosol effects, *J. Clim.*, *22*(6), 1329–1339.

- Polson, D., G. C. Hegerl, R. P. Allan, and B. B. Sarojini (2013a), Have greenhouse gases intensified the contrast between wet and dry regions?, *Geophys. Res. Lett.*, *40*, 4783–4787, doi:10.1002/grl.50923.
- Polson, D., G. C. Hegerl, X. Zhang, and T. J. Osborn (2013b), Causes of robust seasonal land precipitation changes, *J. Clim.*, *26*, 6679–6697.
- Rotstayn, L. D., and U. Lohmann (2002), Tropical rainfall trends and the indirect aerosol effect, *J. Clim.*, *15*(15), 2103–2116.
- Schneider, U., et al. (2014), GPCC's new land surface precipitation climatology based on quality-controlled in situ data and its role in quantifying the global water cycle, *Theor. Appl. Climatol.*, *115*(1-2), 15–40.
- Seager, R., and N. Naik (2012), A mechanisms-based approach to detecting recent anthropogenic hydroclimate change, *Nat. Geosci.*, *1*, 21–24.
- Stevens, B., and G. Feingold (2009), Untangling aerosol effects on clouds and precipitation in a buffered system, *Nature*, *461*, 607–613.
- Trenberth, K., A. Dai, R. Rasmussen, and D. Parsons (2003), The changing character of precipitation, *Bull. Am. Meteorol. Soc.*, *84*(9), 1205–1217.
- Wang, B., et al. (2013), Northern Hemisphere summer monsoon intensified by mega-El Nino/Southern Oscillation and Atlantic multidecadal oscillation, *Proc. Nat. Acad. Sci.*, *110*, 5347–5352.
- Wilcox, L. J., E. J. Highwood, and N. J. Dunstone (2013), The influence of anthropogenic aerosol on multi-decadal variations of historical global climate, *Environ. Res. Lett.*, *8*, 024033.
- Willett, K. M., P. D. Jones, P. W. Thorne, and N. P. Gillett (2010), A comparison of large scale changes in surface humidity over land in observations and CMIP3 GCMs, *Environ. Res. Lett.*, *5*, 025210.
- Wu, P., N. Christidis, and P. Stott (2013), Anthropogenic impact on Earth's hydrological cycle, *Nat. Clim. Change*, *3*(9), 807–810.
- Xie, S.-P., B. Lu, and B. Xiang (2013), Similar spatial patterns of climate responses to aerosol and greenhouse gas changes, *Nat. Geosci.*, *6*(10), 828–832.
- Zhang, R., et al. (2013), Have aerosols caused the observed Atlantic multidecadal variability?, *J. Atmos. Sci.*, *70*, 1135–1144.
- Zhang, X., et al. (2007), Detection of human influence on twentieth-century precipitation trends, *Nature*, *448*(7152), 461–465.